

Direct Fluorescence Monitoring of the Delivery and Cellular Uptake of a Cancer-Targeted RGD Peptide-Appended Naphthalimide Theragnostic Prodrug

Min Hee Lee,[†] Jin Young Kim,[‡] Ji Hye Han,[‡] Sankarprasad Bhuniya,[†] Jonathan L. Sessler,^{§,⊥} Chulhun Kang,^{*,‡} and Jong Seung Kim^{*,†}

[†]Department of Chemistry, Korea University, Seoul, 136-701, Korea

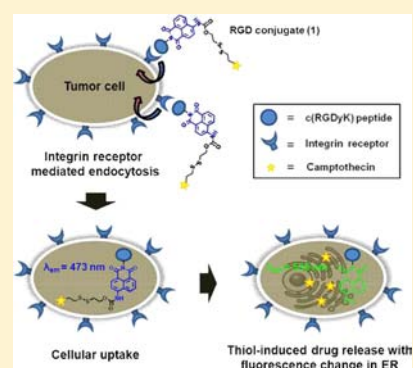
[‡]The School of East-West Medical Science, Kyung Hee University, Yongin, 446-701, Korea

[§]Department of Chemistry and Biochemistry, The University of Texas at Austin, Austin, Texas 78712-0165, United States

[⊥]Department of Chemistry, Yonsei University, 262 Seonsanno Sinchon-dong, Seodaemun-gu, Seoul 120-749, Korea

S Supporting Information

ABSTRACT: Presented here is a multicomponent synthetic strategy that allows for the direct, fluorescence-based monitoring of the targeted cellular uptake and release of a conjugated therapeutic agent. Specifically, we report here the design, synthesis, spectroscopic characterization, and preliminary in vitro biological evaluation of a RGD peptide-appended naphthalimide pro-CPT (compound **1**). Compound **1** is a multifunctional molecule composed of a disulfide bond as a cleavable linker, a naphthalimide moiety as a fluorescent reporter, an RGD cyclic peptide as a cancer-targeting unit, and camptothecin (CPT) as a model active agent. Upon reaction with free thiols in aqueous media at pH 7.4, disulfide cleavage occurs. This leads to release of the free CPT active agent, as well as the production of a red-shifted fluorescence emission ($\lambda_{\text{max}} = 535 \text{ nm}$). Confocal microscopic experiments reveal that **1** is preferentially taken up by U87 cells over C6 cells. On the basis of competition experiments involving okadaic acid, an inhibitor of endocytosis, it is concluded that uptake takes place via RGD-dependent endocytosis mechanisms. In U87 cells, the active CPT payload is released within the endoplasmic reticulum, as inferred from fluorescence-based colocalization studies using a known endoplasmic reticulum-selective dye. The present drug delivery system (DDS) could represent a new approach to so-called theragnostic agent development, wherein both a therapeutic effect and drug uptake-related imaging information are produced and can be readily monitored at the subcellular level. In due course, the strategy embodied in conjugate **1** could allow for more precise monitoring of dosage levels, as well as an improved understanding of cellular uptake and release mechanisms.



INTRODUCTION

In recent years, targeted drug delivery systems have been extensively investigated in an effort to improve chemotherapy treatment regimens.¹ The use of ligands selective for cell-type^{2,3} and conjugation strategies that allow for the selective targeting of a drug have emerged as attractive approaches in this overall context.⁴ Cyclic peptides containing an RGD (Arg-Gly-Asp) sequence are particularly effective targeting agents. These sequences are recognized and internalized by $\alpha_v\beta_3$ integrin,⁵ a well-known tumor-associated receptor. The receptor is highly expressed on activated endothelial cells in several tumors, playing predominant roles in tumor-induced angiogenesis and growth.⁶ In fact, cyclic RGD peptides conjugated with anticancer drugs, such as doxorubicin,⁷ camptothecin,⁸ and paclitaxel,⁹ have been shown to have improved therapeutic activity in vitro and in vivo relative to the corresponding free drugs.^{7–10} Typically, the targeted drug is linked to an RGD carrier with a cleavable linker allowing conversion to the active drug form inside the cells.¹¹ In general, the conclusion that the

drug is taken up and released is operational, being inferred from increased activity or improved cell adhesion, rather than measured directly.^{7–10} This has made it difficult to establish precisely when, where, and how the pharmaceutically active payload is delivered to a cell. It would thus be desirable to develop an RGD-based drug delivery system that contains both an active drug (for efficacy) and a fluorophore (for ease of monitoring uptake and delivery). In principle, this would permit drug delivery and release to be monitored directly. It would also allow the power of theragnostics (combined therapy and diagnostics) to be extended to the subcellular level by enhancing efficacy while facilitating imaging. Here, we report a system that meets these design criteria. Specifically, we detail the design, synthesis, characterization, and optical properties of an RGD peptide-appended naphthalimide pro-camptothecin delivery agent (conjugate **1**), as well as the results of a

Received: April 26, 2012

Published: May 29, 2012

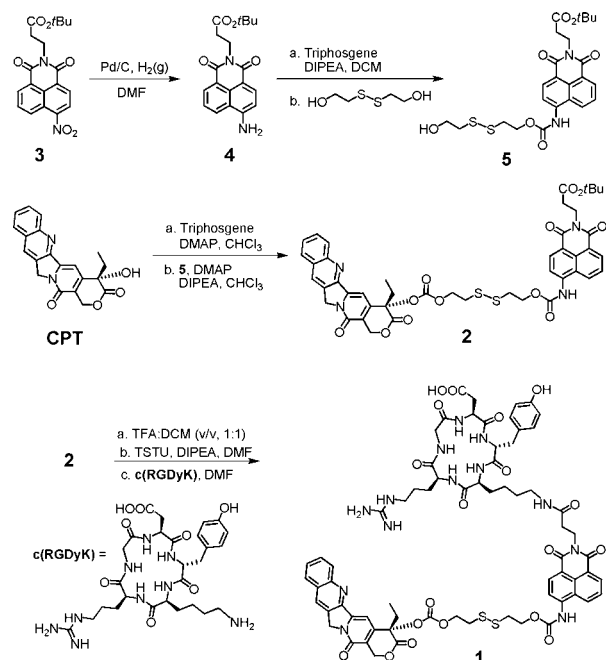
preliminary in vitro biological evaluation using the U87 and C6 cell lines. As detailed below, this multicomponent system shows off-on fluorescence changes that coincide with drug release inside the cells.

RESULTS AND DISCUSSION

Conjugate **1** is composed of camptothecin (CPT), an antitumor inhibitor of topoisomerase I,¹² a disulfide linker cleavable by thiols that are relatively abundant in tumor cells, such as glutathione (GSH) or thioredoxin (Trx),¹³ and a naphthalimide moiety that gives rise to a strong, red-shifted fluorescence signal upon disulfide cleavage.¹⁴ This elaborated system was thus expected to act as an effective drug delivery agent capable of allowing concurrently both selective cell targeting and fluorescent-based monitoring of drug release.

Compound **1** was prepared by the synthetic route outlined in Scheme 1. The naphthalimide derivatives **3–5** were prepared

Scheme 1. Synthetic Route to **1**



by adapting previously published procedures.^{14,15} CPT was reacted with triphosgene followed by treatment with **5** to afford **2** in moderate yield. Hydrolysis of **2** with TFA/DCM, followed by reaction with c(RGDyK), gave the RGD-containing conjugate **1**. The chemical structure of **1** was confirmed by ¹H NMR, ¹³C NMR, MALDI-TOF, and ESI-MS analyses (cf., Supporting Information).

Precursor **2** stands as a convenient RGD-free analogue of **1**. It was used to confirm that cleavage could be effected by treatment with thiols. This was done by treating aqueous solutions of **2** with 0–60 equiv of glutathione (GSH) and monitoring the changes in the absorption and fluorescence spectra. As shown in Figure 1a and 1b, the broad absorption and emission bands at 370 and 473 nm, characteristic of **2**, undergo a red-shift to 430 and 535 nm, respectively, upon treatment with 5.0 mM GSH. The new emission band at 535 nm produced as the result of this treatment corresponds to the 4-aminonaphthalimide derivative **4** (Figure 1c).¹⁴ Importantly, the fluorescence enhancement at 535 nm increases linearly ($R =$

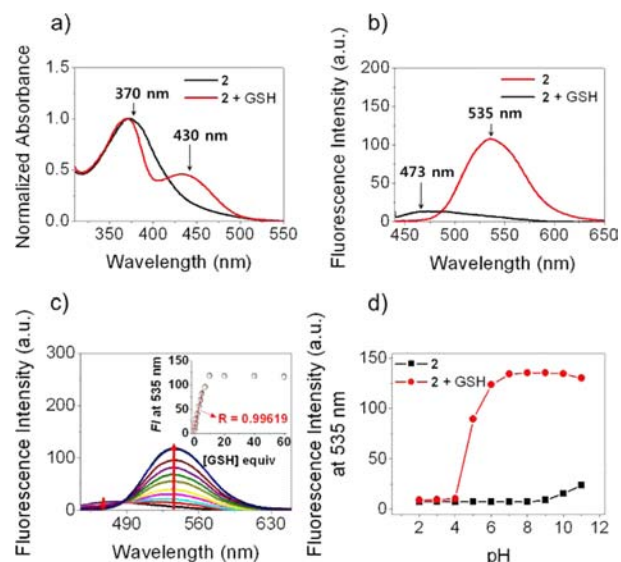


Figure 1. (a) Absorption and (b) fluorescence spectra of **2** (10.0 μ M) recorded in the presence and absence of GSH (5.0 mM). (c) Fluorescence changes of **2** (10.0 μ M) seen upon treatment with increasing concentrations of GSH (0–60 equiv). Inset: Change in fluorescence intensity at 535 nm as a function of GSH concentration. (d) The fluorescence response of **2** (10.0 μ M) with and without GSH (1.0 mM) as a function of pH. All data were acquired 2 h after GSH addition at 37 °C in PBS buffer (pH 7.4) containing 16% (v/v) of DMSO. Excitation was effected at 430 nm.

0.99619) with GSH concentration (0–5 equiv) (see also the inset to Figure 1c).

To evaluate the possibility of interference from other biologically relevant analytes, the reactions of **2** with various thiols, nonthiol amino acids, and metal ions were investigated under the same conditions. Upon the addition of cysteine (Cys) or homocysteine (Hcy) to **2**, similar changes in the absorption and emission features are seen as in the case of GSH (cf., Supporting Information Figures S1 and S2, respectively). On the other hand, no appreciable spectroscopic changes were seen upon exposure to thiol-free amino acids or biologically relevant metal ions.

The pH dependence of the GSH-induced increase in the fluorescence intensity at 535 nm was also investigated. As shown in Figure 1d, in the absence of GSH, compound **2** is stable between pH 2 and 9, whereas in the presence of GSH a large fluorescence enhancement is seen over a pH range of 5–11. Taken in concert, these findings provide support for the notion that the disulfide-linked control system **2** will undergo thiol-induced cleavage in biological milieus but not degrade in the presence of various potential interferants, including metal cations.

Reverse-phase HPLC and ESI-MS analyses were used to confirm the anticipated CPT release as the result of disulfide bond cleavage following exposure to GSH. Under conditions of our analysis, aqueous solutions of **2** give rise to a single peak at 14.3 min in HPLC chromatogram and a major peak at 917.3 m/z corresponding to $[2 + \text{Na}]^+$ in the ESI-MS spectrum (Figure S3, Supporting Information). As can be seen from an inspection of Figure S3a and S3b, in the presence of GSH (0.1 mM), the peak intensity at 14.3 min, corresponding to **2** (0.1 mM), decreases and new strong fragments peaks appear that elute at 10.1 and 11.3 min, respectively. These new fragment peaks are well matched with those from CPT and **4**,

respectively (Figure S4, Supporting Information). In addition, ESI-MS spectral analysis revealed the presence of fragments following exposure of **2** to GSH that are likewise consistent with CPT ($[M - H] = 347.1 m/z$) and **4** ($[M - H] = 339.2 m/z$) (cf., Figure S3c).

Together, these results lead us to suggest that the disulfide bond present in **2** is cleaved by GSH. On the basis of the chemistry involved, this scission is expected to be followed by intramolecular cyclization and cleavage of the neighboring carbamate bond. This, in turn, will serve to release CPT and produce the fluorescent product **4**, as shown in Figure 2. The

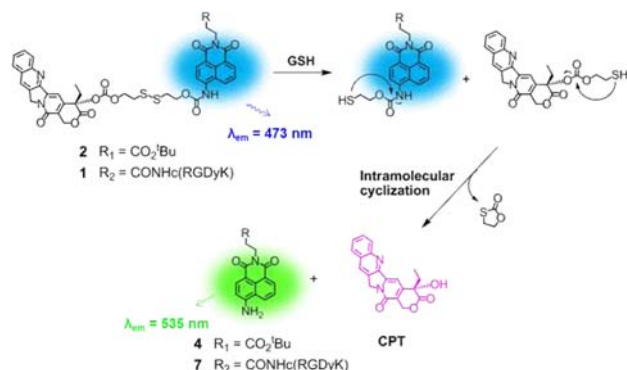


Figure 2. Proposed reaction mechanism of **1** and **2** with GSH under physiological conditions.

fluorescence intensity is thus expected to be directly proportional to the amount of CPT released from **2** (and **1**) as the result of GSH-induced disulfide bond cleavage. Because thiol species, including GSH, are more abundant in tumor cells than in normal cells this release strategy is appealing as an easy-to-monitor drug delivery system (DDS) that, in due course, could prove applicable to cancer therapeutics.¹⁶

To confirm that the pro-CPT RGD-containing conjugate **1** undergoes GSH-induced disulfide cleavage, the reaction of **1** with GSH was tested using conditions identical to those used in the study of **2**. In the case of **1**, the reaction products proved to be the expected free CPT (the payload), as well as the naphthalimide derivative **7**, as inferred from RP-HPLC and ESI-MS analyses (Figure S6, Supporting Information; see also Figure 2 and Scheme S1, Supporting Information). Absorption and fluorescence spectral changes were found to be similar to those of **2** (Figure S5, Supporting Information; see also Figure 1).

Further confirmation that upon disulfide bond cleavage CPT release occurs concurrent with the observed fluorescence changes came from a combined RP-HPLC and fluorimetric time-dependent analysis of conjugate **1**. As can be seen from an inspection of Figure 3, upon treating conjugate **1** with GSH, the amount of CPT released was found to correlate with the observed increase in fluorescence intensity at 535 nm (arising from **7**). In contrast, in the absence of GSH, monitoring solutions of **1** as a function of time revealed neither CPT release nor an enhancement in the fluorescence intensity at 535 nm. We thus consider that the fluorescence changes at 535 nm act as a direct off-on signal that is diagnostic of CPT release.

To demonstrate the role of the RGD moiety in guiding conjugate **1** to $\alpha_v\beta_3$ integrin-rich tumor cells, compounds **1** and **2** were incubated with two different cell lines, namely U87 and C6. These two cell lines were chosen because the expression level of $\alpha_v\beta_3$ integrin in U87 cells is much higher than in C6.¹⁷

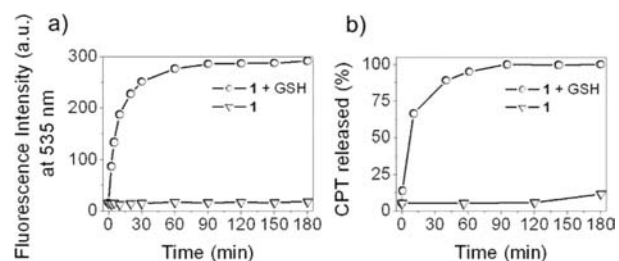


Figure 3. (a) Fluorescence response of **1** (0.1 mM) with and without GSH (0.1 mM). Excitation was effected at 430 nm. (b) CPT released from **1** (0.1 mM) as a function of time in the presence and absence of GSH (0.1 mM). CPT in RP-HPLC chromatograms was detected by UV absorption using 370 nm as the interrogation wavelength. All data were measured at 37 °C in PBS buffer (pH 7.4) containing 16% (v/v) DMSO.

When treated with **1**, a strong increase in the fluorescence intensity was seen in the case of the U87 cells, whereas in the case of the C6 cells only a weak fluorescence signal was seen, even after 60 min incubation (Figure 4). In contrast, analogue

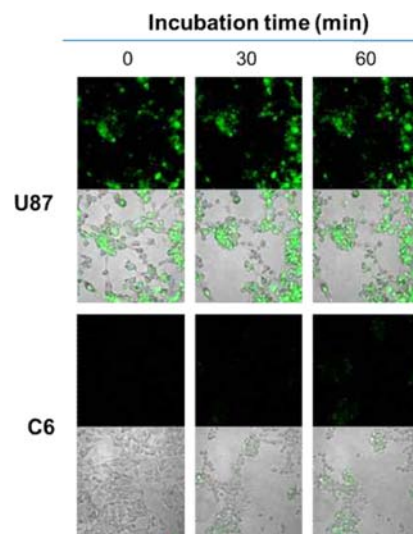


Figure 4. Confocal microscopy images of U87 and C6 cells treated with **1**. The cells were incubated with PBS containing **1** (5 μM), and then the images were obtained at each time point (0, 30, and 60 min). The bottom panels show an overlay of the image with a nonconfocal phase contrast image. Cell images were obtained using excitation at 458 nm and a long-path (>505 nm) emission filter.

2, lacking an RGD-guiding group, displays a strong fluorescence response with essentially identical behavior being seen for both cell lines (Figure S7, Supporting Information). This marked difference in emissive behavior on the case of these two cell lines is consistent with the appealing suggestion, namely that the selective uptake of **1** seen in the case of the U87 cells can be traced to integrin receptor-mediated endocytosis.

To provide further evidence for the proposed endocytic process, the cellular uptake of **1** was studied in the presence of an endocytosis inhibitor, okadaic acid.¹⁸ The results obtained from these studies are shown in Figure 5. We found that the fluorescence intensity of **1** in U87 cells decreases as the concentration of okadaic acid is increased (0–30 nM). In contrast, a strong fluorescence signal was observed for **2** even in the presence of okadaic acid. Considered in conjunction with the results shown in Figures 4 and S7, these findings provide

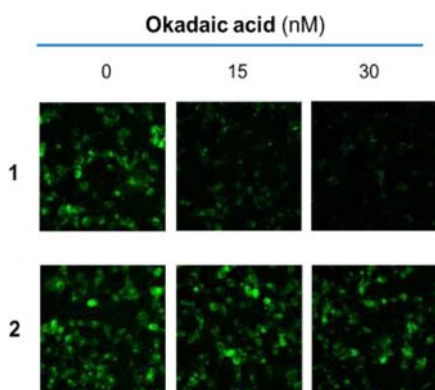


Figure 5. Confocal microscopy images of U87 cells treated with **1** and **2**. The cells were preincubated with media containing okadaic acid (0, 15, and 30 nM) for 30 min at 37 °C. The media were replaced with PBS containing **1** and **2** (5 μ M, respectively) prior to measurement. Cell images were obtained using excitation effected at 458 nm and a long-path (>505 nm) emission filter.

support for the design expectation that cellular uptake into U87 cells occurs via $\alpha_v\beta_3$ integrin-mediated endocytosis. The net result is cell-dependent CPT drug release and off-on fluorescence changes that are ascribed to thiol-induced disulfide bond cleavage.

To identify the cellular location of **1** after $\alpha_v\beta_3$ integrin-mediated endocytosis, colocalization experiments using endoplasmic reticulum (ER), lysosome, and mitochondria-selective staining reagents were performed. As can be seen from an inspection of Figure 6, the fluorescence ascribable to **1** colocalizes well with ERtracker (panel 1-A), but does not match what is observed in the case of Mito- or with LysoTracker (panels 1-B and 1-C). In contrast, the use of **2** gives rise to fluorescence enhancement in the mitochondria (panel 2-C),

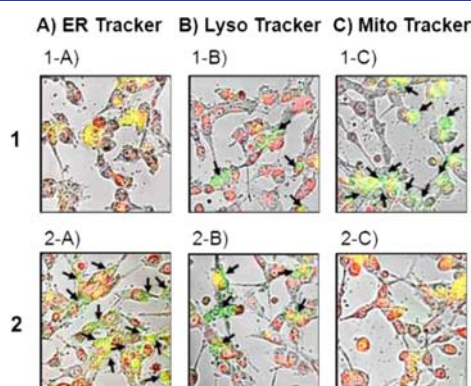


Figure 6. Colocalization studies of **1** and **2** carried out using ER Tracker Red (0.01 μ M) (A) or Lyso Tracker Red DND-99 (0.1 μ M) (B), Mito Tracker Red FM (0.1 μ M) (C) in U87 cells. Panels show overlay of the merged images with the corresponding nonconfocal phase contrast images. The cells were separately pretreated with the trackers in question, and then **1** or **2** (10 μ M, respectively) was added. Fluorescence images of **1** and **2** are labeled with green signals while those of ER-, Mito-, or LysoTracker are labeled with red signals. In the merged image, the yellow regions highlight the colocalized areas of the corresponding dyes, whereas the green colored areas (black arrows) indicate the locations of **1** or **2** alone. Images of the cells were obtained using excitation wavelengths of 458 and 543 nm, and a band-path (505–530 nm, green signal) and a long-path (>585 nm, red signal) emission filters, respectively.

rather than the ER (panel 2-A). Because the ER membrane is contiguous with the inner nuclear membrane (INM), it may be presumed that molecules destined for the INM diffuse through the ER membrane.¹⁹ We, therefore, suggest that thiol-induced disulfide cleavage occurs in the ER in the case of **1**; this cleavage serves to release the CPT molecule, which presumably diffuses into the cell nucleus where it functions as an inhibitor of topoisomerase I.

The efficacy of conjugates **1** and **2**, and thus the inferred level of CPT delivered, was evaluated using standard cell viability protocols. The results are summarized in Figure 7. When the

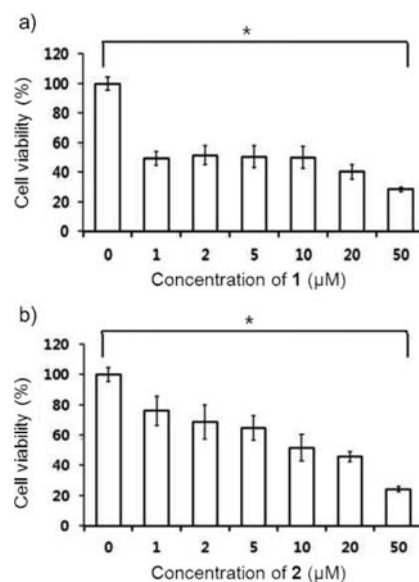
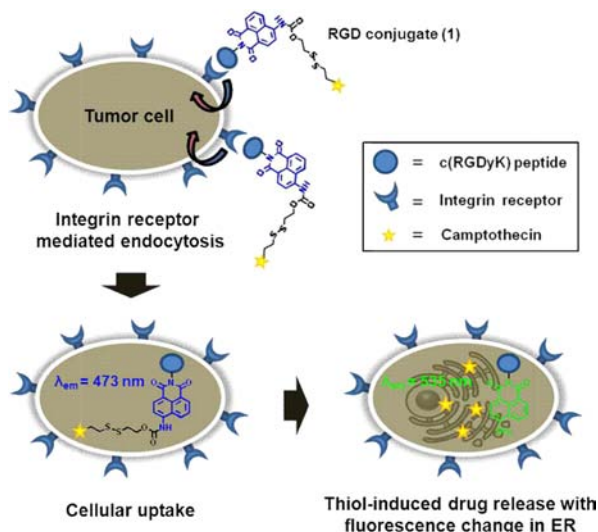


Figure 7. Cell viability of **1** and **2** at different concentrations. The U87 cells were seeded at 1×10^4 cells/well on a 96-well plate. When 80% confluency was reached, the cells were treated with different concentrations of **1** and **2** dissolved in DMEM media for 48 h. After this incubation time, an MTT assay was performed. The data are presented as mean \pm SD ($n = 5$). The statistical significance was marked as * for $p < 0.001$, compared with the normal cells according to Student's t test.

U87 cells were treated with **1** (1.0–50.0 μ M), a dose-dependent decrease in cell viability was clearly observed (49–29% of cell viability in 1.0×10^4 cells/well). The pharmaceutical activity of **1** is evident at 1.0 μ M with a cell viability level of 49% being reached within 48 h (Figure 7a). Conjugate **2** was tested in an analogous manner but gave rise to a lower degree of cytotoxicity (e.g., 76% cell viability at 1.0 μ M after 48 h; Figure 7b). These results are fully consistent with the design expectations and provide experimental support for the suggestion that a major pathway of intracellular delivery of **1** involves integrin receptor-mediated endocytosis. Compound **2** does not benefit from such a localization mechanism and is less active. The superior pharmaceutical activity found for **1** relative to **2** is thus explained by the fact that the CPT released in the ER is more potent than when it is released in the mitochondrion.

The suggested drug delivery mechanism of **1** is shown in Scheme 2. Conjugate **1** selectively penetrates into tumor cells through, presumably, integrin receptor-mediated endocytosis. In the ER, disulfide bond cleavage occurs upon exposure to thiols. This releases the CPT and induces a concomitant fluorescence off-on signal response within the ER. This precise

Scheme 2. The Integrin Receptor Is Highly Expressed on the Surface of Tumor Cells^a



^aThe RGD-containing conjugate **1** is thought to be selectively internalized in the cells by receptor-mediated endocytosis. Upon target-specific internalization, this RGD conjugate (**1**) provides a new fluorescence emission at 535 nm (off-on signal) and releases CPT due to cleavage of the disulfide bond by GSH, a species that is overexpressed in tumor cells (vide supra).

localization leads us to propose that conjugates such as **1** could be used to produce both an imaging and therapeutic effect in various targeted cells. The initial demonstration of this principle, as reported here, thus helps to define what could be a new chapter in theragnostic drug development, namely one where the key elements of sensing and therapy are effectively “miniaturized” such that they function at the cellular level.

CONCLUSIONS

We have described the synthesis, characterization, spectroscopic properties, and biological applications of **1**, an RGD peptide-appended naphthalimide pro-CPT agent. Reaction of **1** with GSH induces disulfide bond cleavage followed by intramolecular cyclization and cleavage of the neighboring carbamate bond. This serves to release the CPT and leads to fluorescence enhancement. From in vitro cellular experiments, we conclude that conjugate **1**, bearing a cyclic RGD peptide subunit, is selectively internalized into the tumor U87 cells via $\alpha_v\beta_3$ integrin-mediated uptake as evidenced by competitive okadaic acid treatment. This uptake permits an off-on observation of the fluorescence changes (signal monitored at 535 nm) upon reaction with GSH (a species overexpressed in cancer cells). In the case of **1**, disulfide bond cleavage occurs in the ER to release the CPT, which in turn diffuses into the nucleus of the U87 cell. This would be an ideal theragnostic delivery system that provides specific tumor targeting and which permits the concentration of free drug to be monitored by fluorescence signaling changes.

EXPERIMENTAL SECTION

β -Ala-O^tBu¹⁵ and naphthalimide derivatives **3**, **4**, and **6**¹⁴ were prepared by procedures reported earlier. Peptide c(RGDyK) was purchased from FutureChem Co., Ltd.

Synthesis of 7. To a mixture of **6** (2.0 mg, 0.7 μ mol) and DIPEA (2.5 μ L, 1.4 μ mol) in DMF (0.5 mL) was added TSTU (1.6 mg, 5.5 μ mol), and the reaction mixture was stirred at room temperature. After 2 h of stirring, c(RGDyK) (4.7 mg, 5.5 μ mol) in DMF was added. The reaction mixture was stirred under nitrogen overnight. The volatile components were removed, and the residue was purified using HPLC (VP-ODS, 4.6 \times 150 mm for the stationary phase; buffer A, H₂O; buffer B, CH₃CN for the mobile phases). Compound **7** was eluted at 5–90% of buffer B for 5–20 min and was lyophilized, affording yellowish fluffy powder (2.0 mg, 33%). The HPLC chromatogram of **7** is shown Figure S19, Supporting Information (>98% purity). HPLC retention time: 9.1 min, ESI-MS m/z (M^+) calcd 885.9, found 886.4 ($M + H^+$).

Synthesis of 5. To a mixture of **4** (1.0 g, 2.9 mmol) and triphosgene (2.6 g, 8.7 mmol) in 20 mL of dry toluene was added DIPEA (1.5 mL, 8.7 mmol) dropwise. The resulting solution was heated at reflux for 3 h. After cooling to room temperature, the reaction mixture was flushed with nitrogen gas. After removal of unreacted phosgene gas (CAUTION: TOXIC) and neutralization in a NaOH bath, a solution of 2,2'-dithiodiethanol (2.3 g, 14.5 mmol) in distilled THF/DCM (v/v, 1:1) was added to the mixture. The reaction mixture was stirred overnight. The solvent was evaporated, at which point CH₂Cl₂ (100 mL) and water (100 mL) were added, and the organic layer was collected. The CH₂Cl₂ layer was dried over anhydrous MgSO₄. After removal of the solvent, the crude product was purified over silica gel using ethyl acetate/hexane (v/v, 1:1) as the eluent to yield **5** as a yellowish oil (91.5 mg, 60%). ESI-MS m/z (M^+) calcd 520.1, found 519.1 ($M - H^+$). ¹H NMR (CDCl₃, 400 MHz): δ 8.54–8.48 (m, 2 H); 8.25 (t, 2 H, $J = 9.6$ Hz); 7.99 (br s, 1 H); 7.69 (t, 1 H, $J = 8.3$ Hz); 4.54 (t, 2 H, $J = 5.9$ Hz); 4.41 (t, 2 H, $J = 7.4$ Hz); 3.96 (br t, 2 H, $J = 5.2$ Hz); 3.06 (t, 2 H, $J = 6.3$ Hz); 2.95 (t, 2 H, $J = 6.0$ Hz); 2.68 (t, 2 H, $J = 7.4$ Hz); 2.56 (br s, 1 H); 1.42 (s, 9 H). ¹³C NMR (CDCl₃, 100 MHz): 170.9, 164.1, 163.6, 153.2, 139.3, 132.6, 131.5, 128.9, 126.7, 123.1, 117.7, 117.1, 81.1, 64.0, 60.7, 41.7, 37.6, 36.4, 34.0, 28.2 ppm

Synthesis of 2. To a mixture of CPT (50 mg, 0.1 mmol) and DMAP (123 mg, 0.7 mmol) in 20 mL of dry chloroform was added triphosgene (0.2 g, 0.5 mmol) dropwise. The resulting solution was heated for 3 h. After being cooled to room temperature, the reaction mixture was flushed with nitrogen gas. After removal of unreacted phosgene gas (CAUTION: TOXIC) and neutralization in a NaOH bath, compound **5** (70 mg, 0.1 mmol), DMAP (35 mg, 0.2 mmol), and DIPEA (25 μ L, 0.1 mmol) were added to the mixture. The reaction mixture was stirred overnight. The solvent was evaporated, at which point CH₂Cl₂ (100 mL) and water (100 mL) were added, and the organic layer was collected. The CH₂Cl₂ layer was dried over anhydrous MgSO₄. After removal of the solvent, the crude product was purified over silica gel using ethyl acetate/hexane (v/v, 4:1) as the eluent to yield **2** as a yellowish solid (60 mg, 47%). ESI-MS m/z (M^+) calcd 894.2, found 923.2 ($M - H^+$). ¹H NMR (CDCl₃, 400 MHz): δ 8.57–8.49 (m, 2 H); 8.38 (s, 1 H); 8.30 (d, 1 H, $J = 8.4$ Hz); 8.22–8.16 (m, 2 H); 8.05 (s, 1 H); 7.95 (d, 1 H, $J = 8.2$ Hz); 7.86–7.82 (m, 1 H); 7.71–7.67 (m, 2 H); 7.32 (s, 1 H); 5.37–5.03 (m, 4 H); 4.58–4.30 (m, 6 H); 3.07–2.95 (m, 4 H); 2.70 (t, 2 H, $J = 7.4$ Hz); 2.27–2.02 (m, 2 H); 1.43 (s, 9 H); 0.98 (t, 3 H, $J = 7.4$ Hz). ¹³C NMR (CDCl₃, 100 MHz): 170.7, 167.4, 164.0, 163.5, 157.1, 153.9, 152.9, 152.1, 148.9, 146.5, 145.6, 139.4, 132.4, 131.3, 130.9, 129.6, 128.9, 128.4, 128.3, 126.8, 126.5, 123.1, 123.0, 117.6, 116.5, 95.9, 80.8, 78.4, 66.9, 66.5, 63.0, 50.0, 37.6, 36.5, 36.3, 33.9, 31.8, 28.1, 7.7 ppm

Synthesis of 1. A solution of TFA/DCM (v/v, 1:1) was added to compound **2** (9 mg, 0.1 mmol). After 30 min of stirring, the volatiles were removed under reduced pressure. The crude product was confirmed by MS analysis (Figure S14, Supporting Information) and then used directly for the next reaction. The crude product was dissolved in DMF (0.5 mL), and DIPEA (3.5 μ L, 0.2 mmol) was added. TSTU (3.0 mg, 0.1 mmol) was then added, and the mixture was stirred at room temperature. After 2 h of stirring, c(RGDyK) (8.5 mg, 0.1 mmol) in DMF was added. The reaction mixture was stirred under nitrogen overnight. Solvent was removed, and the residue was purified using HPLC (C18, 3.5 μ m, 4.6 \times 150 mm for the stationary

phase; buffer A, H₂O containing 0.1% TFA; buffer B, CH₃CN containing 0.1% TFA were used as the mobile phases). Target **1** was eluted at 5–70% of buffer B for 5–30 min and was lyophilized, which afforded a yellowish fluffy powder (8.0 mg, 28%). The HPLC chromatogram of **1** is shown Figure S16, Supporting Information (>97% purity). HPLC retention time: 29.0 min, MALDI-TOF MS m/z (M^+) calcd 1440.5, found 1440.1 (M^+).

Synthetic Materials and Methods. All reactions were carried out under nitrogen atmosphere. Silica gel 60 (Merck, 0.063–0.2 mm) was used for column chromatography. Analytical thin layer chromatography was performed using Merck 60 F254 silica gel (precoated sheets, 0.25 mm thick). ¹H and ¹³C NMR spectra were recorded in CDCl₃ or CD₃OD (Cambridge Isotope Laboratories, Cambridge, MA) on Varian 300 and 400 MHz spectrometers. All chemical shifts are reported in ppm value using the peak of residual proton signals of TMS as an internal reference. Reverse-phase HPLC experiments were conducted using an Agilent HPLC (Agilent 1100 series) with a Zorbax C18 (3.5 μm, 4.6 × 150 mm), Shim-pack VP-ODS (4.6 × 150 mm) column for analytical, Waters HPLC (Waters 600) with XBridge C18 (5 μm, 19 × 150 mm) column for preparative separation. The flow rates for analytical and preparative HPLC were 1.0 mL/min and 6.0 mL/min, respectively. For the mobile phase, buffer A (water with 0.1% v/v TFA) and buffer B (acetonitrile with 0.1% v/v TFA) were used to provide the solvent gradient. ESI mass spectrometric analyses were carried out using an LC/MS-2020 Series (Shimadzu) instrument. MALDI-TOF mass spectral analyses were carried out at the National Center for Interuniversity Research Facilities in Seoul National University.

Spectroscopic Materials and Methods. Stock solutions of biologically relevant analytes [thiols, Val, Tyr, Thr, Tau, Ser, Pro, Phe, Met, Lys, Leu, Ile, His, Gly, Gluc, Glu, Gln, Asp, Asn, Arg, Ala, Trp, Zn(II), Na(I), Mg(II), K(I), Fe(III), Fe(II), Cu(II), and Ca(II)] were prepared in triple distilled water. Stock solutions of **1** and **2** were also prepared in triple distilled water. All spectroscopic measurements were performed under physiological conditions (PBS buffer containing 16% (v/v) of DMSO, pH 7.4, 37 °C). Absorption spectra were recorded on an S-3100 (Scinco) spectrophotometer, and fluorescence spectra were recorded using an RF-5301 PC spectrofluorometer (Shimadzu) equipped with a xenon lamp. Samples for absorption and emission measurements were contained in quartz cuvettes (3 mL volume). Excitation was provided at 430 nm with excitation and emission slit widths of 3 and 1.5 nm, respectively.

Preparation of Cell Cultures. The C6 rat glioma and U87 human glioma cells were maintained and subcultured every other day in DMEM supplemented with 10% fetal bovine serum and 1% penicillin–streptomycin at 37 °C in 5% CO₂ and 95% ir environment. The cells were seeded on 24-well plates and stabilized for overnight. Compounds **1** and **2** were applied to the cells to monitor their uptake and drug release as discussed in the main text above. In some experiments, the cells were incubated with media containing okadaic acid, Mito-, Lyso-, or ERtracker prior to treatment with **1** or **2**. Then the cells were briefly washed with 1 mL of PBS and were then treated with **1** or **2** in PBS. After incubation, residual quantities of **1** or **2** that were not taken up in the cells were removed by washing the cells three times with PBS before the cells were placed in 1 mL of a PBS solution. Fluorescence images were taken using a confocal laser scanning microscope (Zeiss LSM 510, Zeiss, Oberko, Germany).

■ ASSOCIATED CONTENT

📄 Supporting Information

Additional spectra (UV/vis absorption, fluorescence, NMR, ESI-MS) and imaging data and full reference information. This material is available free of charge via the Internet at <http://pubs.acs.org>.

■ AUTHOR INFORMATION

Corresponding Author

kangch@khu.ac.kr; jongskim@korea.ac.kr

Notes

The authors declare no competing financial interest.

■ ACKNOWLEDGMENTS

This work was supported by the CRI project (20120000243) of the National Research Foundation of Korea. J.L.S. thanks the WCU (World Class University) program (R32-2010-000-10217-0) administered through the National Research Foundation of Korea funded by the Ministry of Education, Science and Technology (MEST).

■ REFERENCES

- (1) (a) Garnett, M. C. *Adv. Drug Delivery Rev.* **2001**, *53*, 171–216. (b) Jaracz, S.; Chen, J.; Kuznetsova, L. V.; Ojima, I. *Bioorg. Med. Chem.* **2005**, *13*, 5043–5054. (c) Yokoyama, M. *J. Artif. Organs* **2005**, *8*, 77–84. (d) Torchilin, V. P.; Schäfer-Korting, M. *Handbook of Experimental Pharmacology*; Springer: Berlin, 2010; p 3.
- (2) (a) Olivier, G.; Barbara, S. *Tumor-Associated Antigens: Identification, Characterization, and Clinical Applications*; Wiley-VCH: Weinheim, 2009. (b) Sefah, K.; Shangguan, D.; Xiong, X.; O'Donoghue, M. B.; Tan, W. *Nat. Protoc.* **2010**, *5*, 1169–1185. (c) Quiles, S.; Raisch, K. P.; Sanford, L. J.; Bonner, J. A.; Safavy, A. *J. Med. Chem.* **2010**, *53*, 586–594. (d) Hamann, P. R.; Hinman, L. M.; Beyer, C. F.; Greenberger, L. M.; Lin, C.; Lindh, D.; Menendez, A. T.; Wallace, R.; Durr, F. E.; Upešlacis, J. *Bioconjugate Chem.* **2005**, *16*, 346–353. (e) Boghaert, E. R.; Sridharan, L.; Khandke, K. M.; Armellino, D.; Ryan, M. G.; Myers, K.; Harrop, R.; Kunz, A.; Hamann, P. R.; Marquette, K. *Int. J. Oncol.* **2008**, *32*, 221–234. (f) Krop, I. E.; Beeram, M.; Modi, S.; Jones, S. F.; Holden, S. N.; Yu, W.; Girish, S.; Tibbitts, J.; Yi, J.-H.; Sliwkowski, M. X. *J. Clin. Oncol.* **2010**, *28*, 2698–2704. (g) Landowski, C. P.; Vig, B. S.; Song, X.; Amidon, G. L. *Mol. Cancer Ther.* **2005**, *4*, 659–667. (h) Ramanathan, S.; Pooyan, S.; Stein, S.; Prasad, P. D.; Wang, J.; Leibowitz, M. J.; Ganapathy, V.; Sinko, P. *J. Pharm. Res.* **2001**, *18*, 950–956. (i) No, K.; Lee, J. H.; Yang, S. H.; Cho, M. H.; Kim, M. J.; Kim, J. S. *J. Org. Chem.* **2002**, *67*, 3165–3168.
- (3) (a) Maeda, H.; Seymour, L. W.; Miyamoto, Y. *Bioconjugate Chem.* **1992**, *3*, 351–362. (b) Jain, R. K. *J. Controlled Release* **2001**, *74*, 7–25.
- (4) (a) Chen, X.; Plasencia, C.; Hou, Y.; Neamati, N. *J. Med. Chem.* **2005**, *48*, 1098–1106. (b) Yamazaki, N.; Kojima, S.; Bovin, N. V.; Andre, S.; Gabius, S.; Gabius, H.-J. *Adv. Drug Delivery Rev.* **2000**, *43*, 225–244. (c) Henne, W. A.; Doorneweerd, D. D.; Hilgenbrink, A. R.; Kularatne, S. A.; Low, P. S. *Bioorg. Med. Chem. Lett.* **2006**, *16*, 5350–5355. (d) Russell-Jones, G.; McTavish, K.; McEwan, J.; Rice, J.; Nowotnik, D. *J. Inorg. Biochem.* **2004**, *98*, 1625–1633.
- (5) Pierschbacher, M. D.; Ruoslahti, E. *Nature* **1984**, *309*, 30–33.
- (6) Brooks, P. C.; Clarks, R. A.; Cheresch, D. A. *Science* **1994**, *264*, 569–571.
- (7) (a) Arap, W.; Pasqualini, R.; Ruoslahti, E. *Science* **1998**, *279*, 377–380. (b) de Groot, F. M. H.; Broxterman, H. J.; Adams, H. P. H. M.; van Vliet, A.; Tesser, G. I.; Elderkamp, Y. W.; Schraa, A. J.; Kok, R. J.; Molema, G.; Pinedo, H. M.; Scheere, H. W. *Mol. Cancer Ther.* **2002**, *1*, 901–911.
- (8) (a) Dal Pozzo, A.; Ni, M.-H.; Esposito, E.; Dallavalle, S.; Musso, L.; Bargiotti, A.; Pisano, C.; Vesci, L.; Bucci, F.; Castorina, M.; Foderà, R.; Giannini, G.; Aulicino, C.; Penco, S. *Bioorg. Med. Chem.* **2010**, *18*, 64–72. (b) Dal Pozzo, A.; Esposito, E.; Ni, M.-H.; Muzi, L.; Pisano, C.; Bucci, F.; Vesci, L.; Castorina, M.; Penco, S. *Bioconjugate Chem.* **2010**, *21*, 1956–1967. (c) Huang, B.; Desai, A.; Tang, S.; Thomas, T. P.; Baker, J. R. *Org. Lett.* **2010**, *12*, 1384–1387.
- (9) (a) Chen, X.; Plasencia, C.; Hou, Y.; Neamati, N. *J. Med. Chem.* **2005**, *48*, 1098–1106. (b) Yin, J.; Li, Z.; Yang, T.; Wang, J.; Zhang, X.; Zhang, Q. *J. Drug Targeting* **2011**, *19*, 25–36. (c) Cao, Q.; Li, Z.-B.; Chen, K.; Wu, Z.; He, L.; Neamati, N.; Chen, X. *Eur. J. Nucl. Med. Mol. Imaging* **2008**, *35*, 1489–1498.
- (10) Temming, K.; Schiffelers, R. M.; Molema, G.; Kok, R. J. *Drug Resist. Update* **2005**, *8*, 381–402.
- (11) (a) Han, H. K.; Amidon, G. L. *AAPS Pharmsci.* **2000**, *2*, E6. (b) Rautio, J.; Kumpulainen, H.; Heimbach, T.; Oliyai, R.; Oh, D.;

Jaervinen, T.; Savolainen, J. *Nat. Rev. Drug Discovery* **2008**, *7*, 255–270. (c) Mahato, R.; Tai, W.; Cheng, K. *Adv. Drug Delivery Rev.* **2011**, *63*, 659–670.

(12) (a) Hertzberg, R. P.; Caranfa, M. J.; Hecht, S. M. *Biochemistry* **1989**, *28*, 4629–4638. (b) Hsiang, Y. H.; Liu, L. F.; Wall, M. E.; Wani, M. C.; Nicholas, A. W.; Manikumar, G.; Kirschenbaum, S.; Silber, R.; Potmesil, M. *Cancer Res.* **1989**, *49*, 4385–4389.

(13) (a) Zheng, Z.-B.; Zhu, G.; Tak, H.; Joseph, E.; Eiseman, J. L.; Creighton, D. J. *Bioconjugate Chem.* **2005**, *16*, 598–607. (b) Estrela, J.; Ortega, A.; Obrador, E. *Crit. Rev. Clin. Lab. Sci.* **2006**, *43*, 143–181. (c) Grogan, T. M.; Fenoglio-Prieser, C.; Zehnb, R.; Bellamy, W.; Frutiger, Y.; Vela, E.; Stemmerman, G.; Macdonald, J.; Richter, L.; Gallegos, A.; Powis, G. *Hum. Pathol.* **2000**, *31*, 475–481.

(14) Lee, M. H.; Han, J. H.; Kwon, P.-S.; Bhuniya, S.; Kim, J. Y.; Kang, C.; Kim, J. S. *J. Am. Chem. Soc.* **2012**, *134*, 1316–1322.

(15) Ruijtenbeek, R.; Kruijtzter, J. A. W.; van de Wiel, W.; Fischer, M. J. E.; Flück, M.; Redegeld, F. A. M.; Liskamp, R. M. J.; Nijkamp, F. P. *ChemBioChem.* **2001**, *2*, 171–179.

(16) Gerweck, L. E.; Vijayappa, S.; Kozin, S. *Mol. Cancer Ther.* **2006**, *5*, 1275–1279.

(17) (a) Cai, W.; Wu, Y.; Chen, K.; Cao, Q.; Tice, D. A.; Chen, X. *Cancer Res.* **2006**, *66*, 9673–9681. (b) Zhang, X.; Xiong, Z.; Wu, Y.; Cai, W.; Tseng, J. R.; Gambhir, S. S.; Chen, X. *J. Nucl. Med.* **2006**, *47*, 113–121. (c) Wang, H.; Chen, X. *Expert Opin. Drug Delivery* **2009**, *6*, 745–768.

(18) (a) Hinchliffe, K. A.; Irvine, R. F.; Divecha, N. *EMBO J.* **1996**, *15*, 6516–6524. (b) Higashihara, M.; Takahata, K.; Kurokawa, K.; Ikebe, M. *FEBS Lett.* **1992**, *307*, 206–210. (c) Holen, I.; Gordon, P. B.; Stromhaug, P. E.; Berg, T. O.; Fengsrud, M.; Brech, A.; Roos, N.; Bergs, T.; Seglen, P. O. *Biochem. J.* **1995**, *311*, 317–326.

(19) Saksena, S.; Shao, Y.; Braunagel, S. C.; Summers, M. D.; Johnson, A. E. *Proc. Natl. Acad. Sci. U.S.A.* **2004**, *101*, 12537–12542.